



Topology optimization with wall thickness and piecewise developability constraints for foldable shape-changing structures

Yuqing Zhou¹ · Tsuyoshi Nomura² · Ercan M. Dede¹ · Kazuhiro Saitou³

Received: 20 May 2021 / Revised: 20 February 2022 / Accepted: 3 March 2022 / Published online: 22 March 2022
© The Author(s), under exclusive licence to Springer-Verlag GmbH Germany, part of Springer Nature 2022

Abstract

Foldable shape-changing structures such as origami, deployable, and 4D printed structures have potentials for enhanced packaging, adaptability, and motion capabilities. Distinct geometric features often found in such foldable shape-changing structures include developability and small wall thickness. In this paper, two geometric constraints are introduced to enable the use of density-based topology optimization in designing piecewise developable thin-walled structures. The proposed developability constraint enforces the normal directions of the surfaces of the structures to lie on a prescribed (small) number of input reference planes, which realizes an optimized structure made of piecewise developable surfaces. The proposed thin-wall constraint simultaneously bounds the minimum and the maximum feature sizes in the structures through two PDE-based filtering operations and an aggregation constraint. Several numerical examples demonstrate the effectiveness of the proposed constraints. While the additional constraints inevitably compromise the structural performance, the ability to control the desired geometric features in topology optimization would benefit the rapidly growing field of foldable shape-changing structures.

Keywords Topology optimization · Thin-walled structure · Developability · Geometric constraints

1 Introduction

Foldable shape-changing structures such as origami (Cozmei 2020), deployable (Deleo et al. 2020), and 4D printed structures (Tahouni et al. 2020) have potentials for enhanced packaging, adaptability, and motion capabilities. Distinct geometric features often found in such foldable shape-changing structures include developability and small wall thickness. A developable surface is a surface that can be flattened onto a plane without distortion. Piecewise (near) developability of the surfaces is also necessary for the structures manufactured by flank milling (Stein et al. 2018) and for the

structures manufactured as assemblies of planar materials such as sheet metals, woven composite sheets, and fabrics. The latter also requires structures to be made of geometric features with small, often uniform, wall thickness. Figure 1 shows several examples of foldable shape-changing structures. It is noted that this paper focuses on the geometric design of foldable shape-changing structures as a static problem. The dynamic shape-changing mechanism is out of the scope of this paper.

The current state-of-the-art in computational approaches for designing developable surfaces focus mainly on automatic surface conversion and user-guided interactive design. The automatic surface conversion approach poses the problem as error minimization between the input free-form surface and the converted developable surface. Earlier work has focused on parametric input surfaces, including Bézier (Lang and Röschel 1992; Aumann 2004), B-spline (Elber 1995; Hoschek 1998; Chu and Séquin 2002; Pérez and Suárez 2007; Pottmann 2008) and others (Pottmann and Farin 1995). Recent work focuses on non-parametric input surfaces, including quadrilateral meshes (Julius et al. 2005; Liu et al. 2006; Rabinovich et al. 2018; Jiang et al. 2020), triangle meshes (Mitani and Suzuki 2004; Stein et al.

Responsible Editor: Qing Li

✉ Yuqing Zhou
yuqing.zhou@toyota.com

- ¹ Toyota Research Institute of North America, 1555 Woodridge Ave., Ann Arbor, MI 48105, USA
- ² Toyota Central R&D Labs, Inc., Bunkyo-ku, Tokyo 112-0004, Japan
- ³ Department of Mechanical Engineering, University of Michigan, Ann Arbor, MI 48109, USA

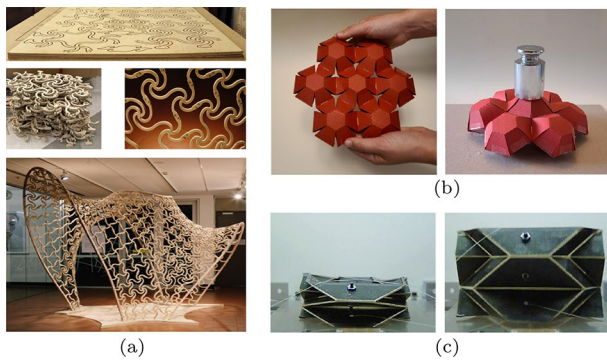


Fig. 1 Examples of foldable shape-changing structures. **a** arbitrarily curved bending-active architectural structure (Laccone et al. 2021); **b** pop-up kirigami structure (Redoutey et al. 2021); and **c** origami-based deployable structure (Deleo et al. 2020)

2018) and others (Shatz et al. 2006; Massarwi et al. 2007; Ion et al. 2020). Since the input surfaces must be given *a priori* for these work, such automatic conversion tools have been used primarily for post-processing of a given design instead of design exploration. The user-guided interactive design approach, on the other hand, employs interactive sketching or CAD tools to realize the real-time interactive editing and conversion of input surfaces to piecewise developable surfaces (Rose et al. 2007; Tang et al. 2016) and to developable surfaces with straight and curved creases (Kilian 2008; Solomon et al. 2012). These tools, however, rely on a human designer to create the input surfaces, and cannot automatically explore alternative surface designs that meet target specifications.

The control of minimum feature sizes is a long-studied topic in density-based topology optimization, originally motivated by the concerns associated with mesh dependency and manufacturability. The spatial average-based low-pass filtering methods have been developed to regularize the sensitivity (Sigmund 1997) and density (Bruns and Tortorelli 2001) fields. Such filters smooth out the density field by limiting the frequency of its spatial variation up to a certain value, indirectly controlling the minimum feature size. Since then, a number of variant methods for the same goal have been developed (Poulsen 2003; Guest et al. 2004; Sigmund 2007; Zhou et al. 2015). The control of maximum feature size, on the other hand, has not been investigated until recently when the needs arose for the control of channel sizes in fluid filters, robustness against localized damage, and thermal gradients and residual stresses. In Guest (2009), local constraints have been used to impose a minimum volume of void in each localized region, indirectly controlling the maximum feature size in the region. This approach was later generalized in a projection-based framework (Carstensen and Guest 2018). An explicit local control of both the maximum and minimum feature sizes

has been proposed using a skeleton-based morphological method (Zhang et al. 2014) and a morphological method with band-pass filtering (Lazarov and Wang 2017). To avoid introducing constraints at each local region within the design domain, an aggregation strategy has been proposed to achieve the goal using only a single constraint (Fernández et al. 2019). Most existing methods, however, require the search of neighbor cells at each design point in each optimization iteration. This is a very computationally expensive operation, especially, for 3D problems (Lazarov and Wang 2017). Alternatively, the neighborhood search could be performed as a preprocessing step, so that the neighbor cell information can be stored and reused. This approach, however, requires significantly more memory utilization and also is impractical for topology optimization using adaptive meshing.

To design 3D thin-walled structures with a uniform wall thickness, several approaches have been independently proposed for different applications. For structures manufactured by deep drawing, a mid surface and sensitivity penalization approach has been proposed (Dienemann et al. 2017). Deep drawing is a process that forms a planar sheet metal blank to the shape of a mold by a mechanical press. While the optimized results are very suitable for the deep drawing applications, the extension to generic thin-walled structures is not straightforward, since the approach requires a prescribed press direction as an input. For structures made of solid thin coating enclosing infill materials, the spatial gradient of the density field processed with a series of filtering and projection has been used to achieve a uniform coating thickness (Clausen et al. 2015, 2015). This approach, however, is also not deemed applicable to generic thin-walled structures because infill materials are required to extract the coating. It is also not possible to have branches and holes in the coating. For structures assembled of plates with uniform thickness, a geometric projection method has been proposed (Zhang et al. 2016, 2017, 2018), where each plate is explicitly represented by its shape and location design variables. While curved plates and holes can be attained by introducing additional design variables, the geometry attainable by this method is rather limited since they are limited by the number and type of plates considered.

This paper proposes two geometric constraints to design *piecewise developable thin-walled* structures for use with density-based topology optimization. The proposed constraint on surface developability enforces the directions of the surface normal, namely the spatial gradient of the density field near the transition to void, to lie on a (small) number of input reference planes. While this conservative constraint only imposes the sufficient condition for piecewise developability, it is far more computationally efficient than a necessary and sufficient developability constraint based on the Gaussian curvature, which makes it highly suitable

for use with density-based topology optimization. To design generic thin-walled structures containing branches and holes without assuming any specific manufacturing processes, the proposed constraint on (small) uniform wall thickness enforces the bounds on the minimum and maximum feature sizes, while iteratively narrowing the gap between them during optimization. This constraint on uniform wall thickness is implemented with a Helmholtz PDE filter (Lazarov and Sigmund 2011; Kawamoto 2011) for the minimum feature size control, and another Helmholtz PDE filter and an aggregation constraint for the maximum feature size control. The PDE-based filters are chosen since they do not require information about neighbor cells, which is especially convenient for problems with unstructured mesh and adaptive meshing. It is noted that while adaptive 3D tetrahedral elements are used in all numerical examples presented in this paper, the proposed two constraints are mesh independent, which can be applied to any 2D or 3D, fixed or adaptive mesh types.

The rest of the paper is organized as follows. Section 2 introduces the mathematical formulation of the piecewise developability constraint and the thin-wall constraint. Section 3 formulates the topology optimization problem with these constraints. Section 4 presents several numerical examples demonstrating the topology optimization with the proposed constraints. Section 5 summarizes the current study and opportunities for future research.

2 Piecewise developability and thin-wall constraints

2.1 Design field regularization

Our proposed constraints on piecewise surface developability and wall thickness are defined as functions of the regularized design field in the density-based topology optimization. In a design domain Ω , a scalar design field $\phi : \Omega \mapsto [-1, 1]$ is defined to represent the material domain Ω_d to be optimized:

$$H(\phi(\mathbf{x})) = \begin{cases} 0 & \text{for } \forall \mathbf{x} \in \Omega \setminus \Omega_d, \\ 1 & \text{for } \forall \mathbf{x} \in \Omega_d, \end{cases} \tag{1}$$

where \mathbf{x} stands for a design point in Ω and $H : \mathbb{R} \mapsto \{0, 1\}$ is the Heaviside function. A Helmholtz PDE filter (Lazarov and Sigmund 2011; Kawamoto 2011) is used to regularize the design field ϕ :

$$-\underline{r}^2 \nabla^2 \tilde{\phi} + \tilde{\phi} = \phi, \tag{2}$$

where \underline{r} is the minimum feature radius. Then fictitious material density field ρ can be defined by a smoothed Heaviside function $\tilde{H} : \mathbb{R} \mapsto [0, 1]$:

$$\rho(\tilde{\phi}) = \begin{cases} 0 & \text{for } \tilde{\phi} < -\tilde{h}, \\ \tilde{H}(\tilde{\phi}) & \text{for } -\tilde{h} \leq \tilde{\phi} \leq \tilde{h}, \\ 1 & \text{for } \tilde{\phi} > \tilde{h}, \end{cases} \tag{3}$$

where

$$\tilde{H}(\tilde{\phi}) = \frac{1}{2} + \frac{15}{16} \left(\frac{\tilde{\phi}}{\tilde{h}}\right) - \frac{5}{8} \left(\frac{\tilde{\phi}}{\tilde{h}}\right)^3 + \frac{3}{16} \left(\frac{\tilde{\phi}}{\tilde{h}}\right)^5. \tag{4}$$

It is noted that all smoothed Heaviside functions used in the rest of this paper including \tilde{H} and \hat{H} follow the same formulation with different h parameter settings.

2.2 Piecewise developability constraint

Mathematically, a developable surface is a smooth surface with zero Gaussian curvature (Kühnel 2015). If a surface is made only of multiple patches of developable surfaces, it is said to be piecewise developable. A piecewise developable surface can consist of patches of planar surfaces, cylinders, cones, and tangent surfaces.

Gaussian curvature K_g for an implicit surface S is given as (Goldman 2005):

$$K_g = \frac{\nabla S \mathbf{H}^*(S) \nabla S^T}{|\nabla S|^4}, \tag{5}$$

where ∇S is the gradient and $\mathbf{H}^*(S)$ is the adjoint of the Hessian. The numerical computation of the second derivatives in \mathbf{H}^* poses significant challenge in terms of time, accuracy, and stability of computation. As a result, the Gaussian curvature in Eq. 5 poses an extreme challenge for use within the gradient-based topology optimization. To alleviate the challenge associated with direct Gaussian curvature computation, this paper proposes a much simpler sufficient condition for surface developability, which depends only on the surface normal (*i.e.*, ∇S) and hence far more computationally viable than a generic constraint based on the Gaussian curvature.

Namely, the proposed piecewise developability constraint uses the criterion that the normal directions of a surface lie on a (small) number of input reference planes. Such a surface is indeed a developable surface, since a surface patch with its normal directions lie on the same plane is developable. There are, however, developable surfaces that do not meet the criterion, *e.g.*, cones and tangent surfaces. This criterion therefore is a sufficient but not necessary condition for piecewise developability. The constraint is mathematically stated as:

$$\int_{\Omega} \prod_{k=1}^K (\mathbf{v}^{(k)} \cdot \nabla \tilde{\phi})^2 d\Omega - \bar{\epsilon} \leq 0, \tag{6}$$

where $\mathbf{v}^{(k)}, k = 1, \dots, K$ is the normal vector of K the input reference planes, $\bar{\epsilon}$ is a positive infinitesimal number, and $\nabla\tilde{\phi}$ is the spatial gradient of the regularized design field:

$$\nabla\tilde{\phi} = \left(\frac{\partial\tilde{\phi}}{\partial x}, \frac{\partial\tilde{\phi}}{\partial y}, \frac{\partial\tilde{\phi}}{\partial z} \right). \tag{7}$$

It is noted that the spatial gradient is evaluated on $\tilde{\phi}$, not on ρ , for numerical stability. Eq. 6 is satisfied only if $\nabla\tilde{\phi} \neq 0$ and is approximately perpendicular to one of the normal vectors of the input reference planes. Since $\nabla\tilde{\phi} \approx 0$ within the material and void regions during topology optimization, Eq. 6 effectively works to constrain the transition regions between the material and void, which can be seen as a relaxation of structural surfaces.

While Eq. 6 is only a sufficient condition of piecewise developability, it does constrain the surfaces of the structure to be curvilinear patches of planes and cylindrical surfaces with the curvatures lie on one of the K input reference planes. Since planes and cylindrical surfaces constitute a majority of developable surfaces (Kilian 2008), it is hypothesized that the surface topography achievable by Eq. 6 would be reasonably rich, with added benefit of tunable computational complexity by means of the input reference planes.

2.3 Thin-wall constraint

The uniform small thickness in the optimized structure is achieved by simultaneously constraining the minimum and maximum feature sizes while iteratively narrowing the gap between them during optimization. This will overcome the limitations in the previous approaches for thin-walled structure design by allowing the exploration of generic wall topology containing branches and holes without assuming any specific manufacturing processes. It is noted that a similar concept has been applied to the topology optimization of 2D truss-like structures with uniform member widths (Niu and Wadbro 2019). The constraint is implemented with a Helmholtz PDE filter (Lazarov and Sigmund 2011; Kawamoto 2011), originally applied for the minimum feature size control, and another Helmholtz PDE filter and an aggregation constraint for the maximum feature size control. Conceptually, the proposed PDE-based method shares a similar trait to previously reported works on the maximum feature size control method (Guest 2009) and the lattice infill method (Wu et al. 2017, 2018). The primary advantage of the proposed PDE-based method is that the information about neighbor cells is not required, which makes it especially advantageous to problems with unstructured mesh and adaptive meshing as addressed in this paper.

The minimum feature radius \underline{r} in Eq. 2 controls the minimum feature size in the regularized design field $\tilde{\phi}$, where the relation between \underline{r} and the filter radius \underline{R} in

the standard spatial average-based filtering methods is (Clausen et al. 2015):

$$\underline{r} = \frac{\underline{R}}{2\sqrt{3}}. \tag{8}$$

Therefore, the material design field ρ , obtained from $\tilde{\phi}$ using Eq. 3, has no features smaller than \underline{R} .

The maximum feature size is indirectly controlled by exploiting a general mathematical property of Helmholtz PDE filters, where for the input field bounded in $[0, 1]$, the regularized field exceeds 1 *only when* the input field has features larger than the multiplier to Laplacian. This means, the maximum feature size can be imposed on the material density field (which is bounded in $[0, 1]$ by 1) filtering it with another Helmholtz PDE filter and 2) constraining the regularized field to be less than 1 in the entire design domain. Instead of filtering ρ , however, a separate density field $\tilde{\rho}$ is created from the regularized design field $\tilde{\phi}$:

$$\tilde{\rho}(\tilde{\phi}) = \begin{cases} 0 & \text{for } \tilde{\phi} < -\bar{h}, \\ \bar{H}(\tilde{\phi}) & \text{for } -\bar{h} \leq \tilde{\phi} \leq \bar{h}, \\ 1 & \text{for } \tilde{\phi} > \bar{h}, \end{cases} \tag{9}$$

where a Heaviside function \bar{H} is different from \hat{H} . This separation of the density field for geometric analysis ($\tilde{\rho}$) from the one for structural analysis (ρ) helps maintain numerical stability. During the course of optimization, a continuation scheme on \bar{h} can be applied to Eq. 3 to avoid premature convergence to a local minimum while a narrow Heaviside bandwidth \bar{h} can be applied to Eq. 9 to ensure the satisfaction of geometric constraints at all iterations.

The density field ($\tilde{\rho}$) is then regularized by a Helmholtz PDE with filter radius $\bar{r} > \underline{r}$ to produce the regularized density $\bar{\rho}$:

$$-\bar{r}^2 \nabla^2 \bar{\rho} + \bar{\rho} = \tilde{\rho}. \tag{10}$$

Similar to Eq. 8, \bar{r} can be linked with the actual geometric feature size \bar{R} . Rather than introducing many local constrains (Guest 2009) or a P-norm aggregation constraint (Wu et al. 2017, 2018) to bound the maximum feature size, this paper follows a numerically robust aggregation method based on smoothed Heaviside projection, which has been successfully applied to the stress-constrained topology optimization (Wang and Qian 2018):

$$\int_{\Omega} \hat{H}(\bar{\rho} - \beta, \hat{h}) \left(\frac{\bar{\rho}}{\beta} \right)^{\eta} d\Omega - \bar{\epsilon} \leq 0, \tag{11}$$

where β is the prescribed upper bound of $\bar{\rho}$, \hat{h} is the smoothed Heaviside bandwidth parameter, η is the penalty factor, $\bar{\epsilon}$ is a positive infinitesimal number.

In order to precisely bound the maximum feature size to be \bar{R} , upper bound β should be set to a value smaller than yet very close to 1, and \hat{h} should be set to an infinitesimal value. However, this setting is not practical for the sensitivity-driven numerical optimization due to the lack of smoothness in the Heaviside function \hat{H} . To resolve this numerical challenge, a filter radius larger than the desired maximum feature size should be used in Eq. 10 so that moderate values for β and \hat{h} can be used. With the appropriate settings of \underline{r} and \bar{r} (or equivalently \underline{R} and \bar{R}), both the minimum and maximum feature sizes can be indirectly controlled. In order to achieve the uniform feature size control, both feature size radius parameters can be set as identical. However, this will lead to the numerical challenge for the maximum feature size constraint Eq. 11. For this reason, the values of \underline{r} and \bar{r} are set as apart initially (with $\underline{r} < \bar{r}$, of course) and updated during optimization, so the gap between them is iteratively reduced to a sufficiently small value at convergence.

Figure 2 illustrates simple numerical tests to gain insights towards the appropriate settings for \underline{r} , \bar{r} , β , and \hat{h} . Figure 2a shows a sample input $\bar{\rho}$ field, where the four strips have thicknesses (from top to bottom) $4R$, $2R$, R , and $0.5R$, respectively. It is generally recommended that tight bandwidth is set in Eq. 9 so that $\bar{\rho}$ is almost 0 or 1 everywhere. It should be noted that the bottom strip has the thickness smaller than R , which should not be present in the actual optimization runs due to Eqs. 2 and 3. Figure 2b–d show, from left to right, the $\bar{\rho}$ fields with \bar{R} of $4R$, $2R$, and $1.5R$, respectively. With the decrease of \bar{R} (or equivalently \bar{r}), the values of the strips thicker than \bar{R} increase, indicating the detection of these strips by means of

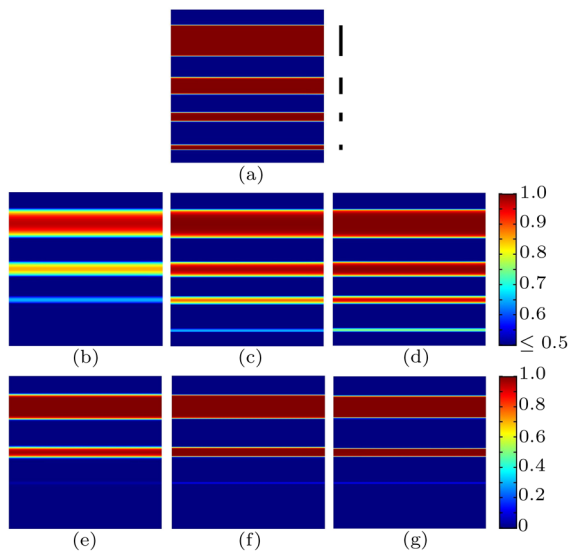


Fig. 2 Test of filter setting for the maximum feature size control. **a** sample input $\bar{\rho}$ field with strips with (from top to bottom) $4R$, $2R$, R , and $0.5R$ thick, **b–d** $\bar{\rho}$ fields with \bar{R} of $4R$, $2R$, and $1.5R$, **e–g** $\hat{H}(\bar{\rho} - \beta, \hat{h})$

higher values of $\bar{\rho}$. Figure 2e–g show, from left to right, the $\hat{H}(\bar{\rho} - \beta, \hat{h})$ fields with (β, \hat{h}) of $(0.75, 0.2)$, $(0.90, 0.05)$, and $(0.97, 0.015)$, respectively. With the larger $\bar{R} - \underline{R}$ (or equivalently $\bar{r} - \underline{r}$), smaller values of β and larger values of \hat{h} , which corresponds to smoother Heaviside functions, can be used to effectively filter out the strips thinner than \bar{R} in order for Eq. 11 to penalize only the strips thicker than \bar{R} . The profiles of the smoothed Heaviside functions to generate Fig. 2e–g are plotted in Fig. 3. The function smoothness indeed improves with smaller β and larger \hat{h} settings. It is noted while these tests can provide some insights towards the relationship between the filter radii and the bandwidth of smoothed Heaviside function to achieve a uniform feature size, the actual settings may vary in different topology optimization problems.

3 Optimization formulation

The structural topology optimization problem with the piecewise developability constraint and the thin-wall constraint is summarized as follows:

$$\begin{aligned}
 &\text{minimize: } F \\
 &\quad \phi \\
 &\text{subject to: } g_1 := \int_{\Omega} \frac{\rho}{V_0} d\Omega - \bar{V} \leq 0 \\
 &\quad g_2 := \int_{\Omega} \prod_{k=1}^K (\mathbf{v}^{(k)} \cdot \nabla \tilde{\phi})^2 d\Omega - \bar{\epsilon} \leq 0 \\
 &\quad g_3 := \int_{\Omega} \hat{H}(\bar{\rho} - \beta, \hat{h}) \left(\frac{\bar{\rho}}{\beta}\right)^{\eta} d\Omega - \bar{\epsilon} \leq 0 \quad (12) \\
 &\quad \text{equilibrium equations} \\
 &\quad \text{material interpolation equation} \\
 &\quad \phi \in [-1, 1]^{\Omega}
 \end{aligned}$$

where the transformations from ϕ to ρ and to $\bar{\rho}$ are detailed in Eqs. 2-3 and Eqs. 9-10, respectively, and summarized in Fig. 4. Function F is the structural performance objective. Function g_1 is the volume fraction constraint where V_0 is the total volume of the design domain, and \bar{V} is the prescribed maximum allowable volume fraction. Functions g_2 and g_3 are the developability constraint (Eq. 6) and the thin-wall constraint (Eq. 11), respectively.

For a structural compliance minimization problem, objective function F is defined as:

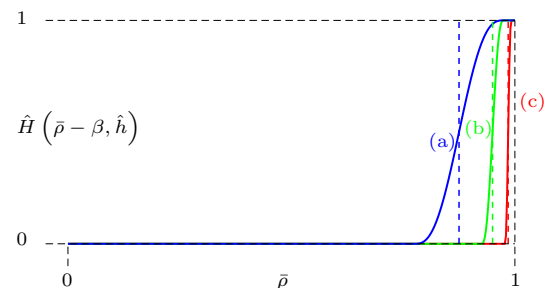


Fig. 3 Smoothed Heaviside functions with different bandwidth parameters (β, \hat{h}) : **a** $(0.75, 0.2)$, **b** $(0.90, 0.05)$ **c** $(0.97, 0.015)$

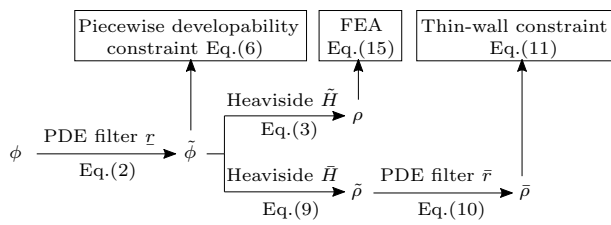


Fig. 4 Transformations of field variables

$$F = \int_{\Omega} \frac{1}{2} \boldsymbol{\sigma}^T \boldsymbol{\epsilon} d\Omega, \tag{13}$$

and equilibrium equations can be given, for example, as:

$$\begin{aligned} \nabla \cdot \boldsymbol{\sigma} &= \mathbf{0} \text{ in } \Omega \\ \mathbf{u} &= \mathbf{0} \text{ on } \Gamma_d, \\ \boldsymbol{\sigma} \cdot \mathbf{n} &= \mathbf{t} \text{ on } \Gamma_n \end{aligned} \tag{14}$$

where $\boldsymbol{\sigma} = \mathbf{C} \cdot \boldsymbol{\epsilon}(\mathbf{u})$ is the stress field, $\boldsymbol{\epsilon}(\mathbf{u})$ is the strain field. \mathbf{C} is the elasticity tensor, Γ_d is the Dirichlet boundary, and Γ_n is the Neumann boundary.

The elasticity tensor \mathbf{C} is obtained in material interpolation equation, which for example, can be the SIMP power law:

$$\mathbf{C} = \mathbf{C}_v + \rho^P (\mathbf{C}_s - \mathbf{C}_v), \tag{15}$$

where \mathbf{C}_s and \mathbf{C}_v are the full solid elasticity tensor and void tensor, respectively, ρ is the regularized material density, and P is the penalization parameter.

The sensitivity calculation of objective function F follows the chain rule as follows:

$$\frac{\partial F}{\partial \phi} = \frac{\partial}{\partial \phi} (F \circ \rho \circ \tilde{\phi})(\phi) = \frac{\partial F}{\partial \rho} \frac{\partial \rho}{\partial \tilde{\phi}} \frac{\partial \tilde{\phi}}{\partial \phi}, \tag{16}$$

where a standard adjoint method (Bendsoe and Sigmund 2003) is used to compute $\frac{\partial F}{\partial \rho}$. For the linear elastic system written as $\mathcal{K}\mathbf{u} = \mathbf{f}$, the Lagrangian can be defined as follows,

$$\mathcal{L}(\mathbf{u}, \rho, \lambda) = F(\mathbf{u}, \rho) + \lambda^T (\mathcal{K}\mathbf{u} - \mathbf{f}), \tag{17}$$

where λ is the Lagrange multipliers. As $(\mathcal{K}\mathbf{u} = \mathbf{f})$ represents the physics equilibrium, any λ can be chosen to satisfy $\mathcal{L} = F$. Its gradient can be computed as follows:

$$\begin{aligned} \frac{\partial F}{\partial \rho} &= \frac{\partial \mathcal{L}}{\partial \rho} \\ &= \frac{\partial F}{\partial \rho} + \frac{\partial F}{\partial \mathbf{u}} \frac{\partial \mathbf{u}}{\partial \rho} + \lambda^T \left(\frac{\partial \mathcal{K}}{\partial \rho} \mathbf{u} + \mathcal{K} \frac{\partial \mathbf{u}}{\partial \rho} \right) \\ &= \frac{\partial F}{\partial \rho} + \lambda^T \frac{\partial \mathcal{K}}{\partial \rho} \mathbf{u} + \left(\frac{\partial F}{\partial \mathbf{u}} + \lambda^T \mathcal{K} \right) \frac{\partial \mathbf{u}}{\partial \rho}. \end{aligned} \tag{18}$$

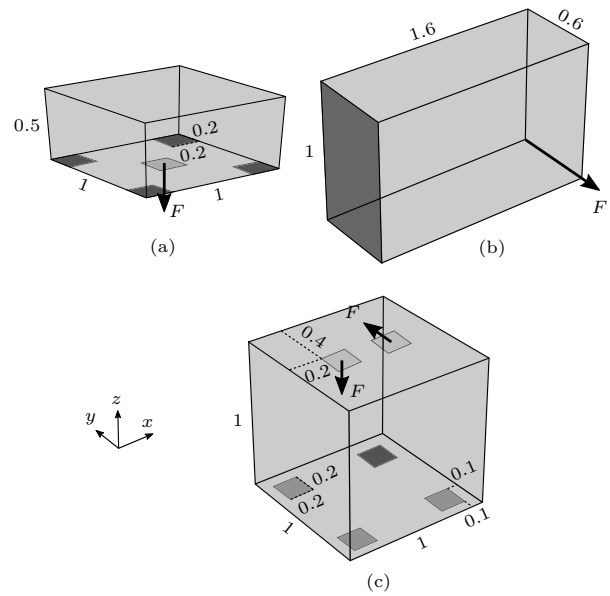


Fig. 5 Design domains and boundary conditions for the examples of **a** center loaded cuboid, **b** sheared cantilever beam, and **c** multiply loaded cube

To avoid calculating $\frac{\partial \mathbf{u}}{\partial \rho}$, λ is chosen as $\frac{\partial F}{\partial \mathbf{u}} + \lambda^T \mathcal{K} = 0$, which is also known as the adjoint equation.

Sensitivity calculation of all constraints g_1, g_2 and g_3 also follows the chain rule as follows:

$$\frac{\partial g_1}{\partial \phi} = \frac{\partial}{\partial \phi} (g_1 \circ \rho \circ \tilde{\phi})(\phi) = \frac{\partial g_1}{\partial \rho} \frac{\partial \rho}{\partial \tilde{\phi}} \frac{\partial \tilde{\phi}}{\partial \phi}, \tag{19a}$$

$$\frac{\partial g_2}{\partial \phi} = \frac{\partial}{\partial \phi} (g_2 \circ \tilde{\phi})(\phi) = \frac{\partial g_2}{\partial \tilde{\phi}} \frac{\partial \tilde{\phi}}{\partial \phi}, \tag{19b}$$

$$\frac{\partial g_3}{\partial \phi} = \frac{\partial}{\partial \phi} (g_3 \circ \bar{\rho} \circ \tilde{\phi})(\phi) = \frac{\partial g_3}{\partial \bar{\rho}} \frac{\partial \bar{\rho}}{\partial \tilde{\phi}} \frac{\partial \tilde{\phi}}{\partial \phi}. \tag{19c}$$

4 Numerical examples

This section presents three design examples: a center loaded cuboid, a sheared cantilever beam, and a multiply loaded cube. Their design domains and boundary conditions are presented in Fig. 5. The optimization problem in Eq. 12 is solved by the method of moving asymptotes (Svanberg 1987). The equilibrium equations are solved by a finite element method, and the sensitivity is computed following the chain rule and a standard adjoint method, both using COMSOL Multiphysics. In each example, the design field is uniformly initialized so that the volume fraction constraint

g_1 is active at the beginning of optimization. The optimization terminates when the change in the objective function becomes sufficiently small or the prescribed number of iterations is reached, whichever comes first.

4.1 Volumetric structure with piecewise developable surfaces

The first example, a center loaded cuboid, demonstrates the proposed piecewise developability constraint. As seen in Fig. 5a, the design domain is subject to a unit downward force applied at the center of the bottom face, whose four corners are fixed in all degrees of freedom. The maximum allowable volume fraction is set as 35%. As a baseline for comparison, the optimized design using the conventional SIMP topology optimization (without geometric constraints) is presented in Fig. 6. It is observed that the optimized design has a star-like overall geometry with a curved surface with no visible edge. The resulting structural compliance is normalized as 1.00 for comparison.

Figure 7 presents the optimized design using the proposed piecewise developability constraint with two normal vectors of input reference planes, $\mathbf{v}^{(1)} = (1, 0, 0)$ and $\mathbf{v}^{(2)} = (0, 1, 0)$. Its normalized structural compliance is 1.04, namely 4% performance degradation compared with the baseline design without the developability constraint. While it shares the overall star-like shape with the baseline, the optimized structure appears to be made of singly curved surfaces connected by visible edges. Figure 8 verifies that the surface normal directions are indeed perpendicular to at least one of the input normal vectors of the two reference planes.

The optimized design in Fig. 7 is fabricated with 3D printing. Its surface is flattened into a 2D pattern, which is printed on a paper and cut. As demonstrated in Fig. 9, the

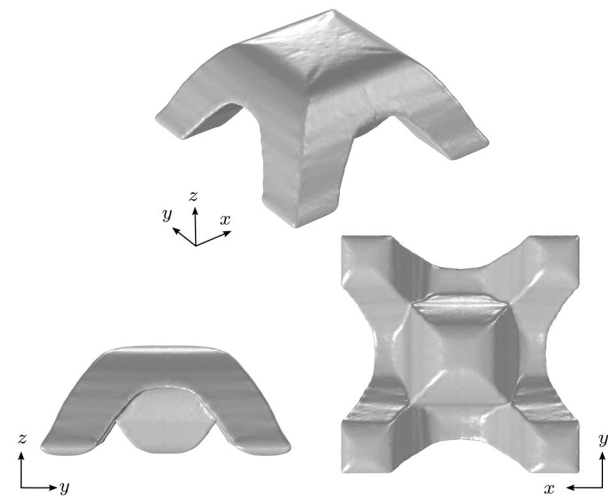


Fig. 7 Optimized structure with the piecewise developability constraint with $\mathbf{v}^{(1)} = (1, 0, 0)$ and $\mathbf{v}^{(2)} = (0, 1, 0)$. Structural compliance = 1.04 (normalized)

2D pattern can be taped to the surface of the printed solid volumetric part without stretching, wrinkling and tearing.

Another optimized structure is presented in Fig. 10 with a different set of the input vectors $\mathbf{v}^{(1)} = (\sqrt{2}/2, \sqrt{2}/2, 0)$ and $\mathbf{v}^{(2)} = (\sqrt{2}/2, -\sqrt{2}/2, 0)$. Its resulting structural compliance is 1.06 (normalized). The optimized structure again has an overall star-like shape, but with vastly different surface construction from that of the prior two designs. Figure 11 verifies that the surface normal directions are perpendicular to at least one of the prescribed input vectors.

While this example demonstrated the case with only two input vectors, the proposed piecewise developability

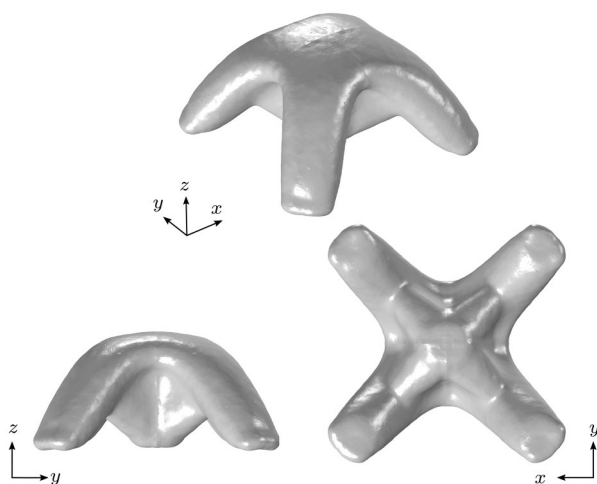


Fig. 6 Baseline structure using the conventional SIMP topology optimization. Structural compliance = 1.00 (normalized)

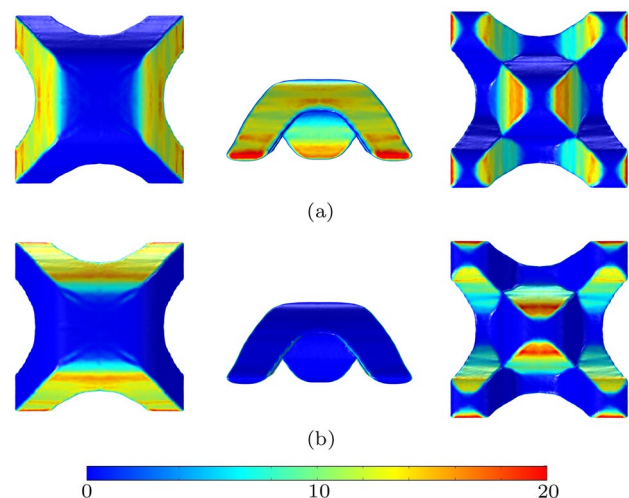


Fig. 8 Verification of the piecewise developability constraint for Fig. 7 design: **a** $(\nabla\phi \cdot \mathbf{v}^{(1)})^2$ and **b** $(\nabla\phi \cdot \mathbf{v}^{(2)})^2$



Fig. 9 The prototype demonstration of taping a 2D pattern to the surface of an optimized and printed solid volumetric part

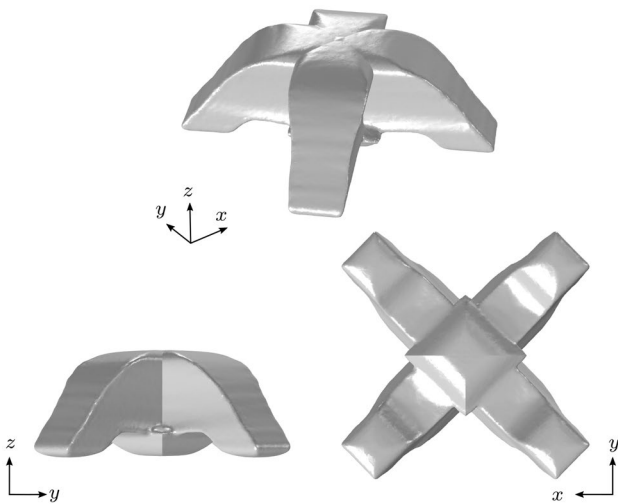


Fig. 10 Optimized structure with the piecewise developability constraint with $\mathbf{v}^{(1)} = (\sqrt{2}/2, \sqrt{2}/2, 0)$ and $\mathbf{v}^{(2)} = (\sqrt{2}/2, -\sqrt{2}/2, 0)$. Structural compliance objective = 1.06 (normalized)

constraint should be readily applicable to designing structures with more input vectors. It is noted that the input vectors can also be simultaneously optimized with the design of structures by appropriately parameterizing their orientations to avoid the 2π periodicity (Nomura 2019; Zhou et al. 2021).

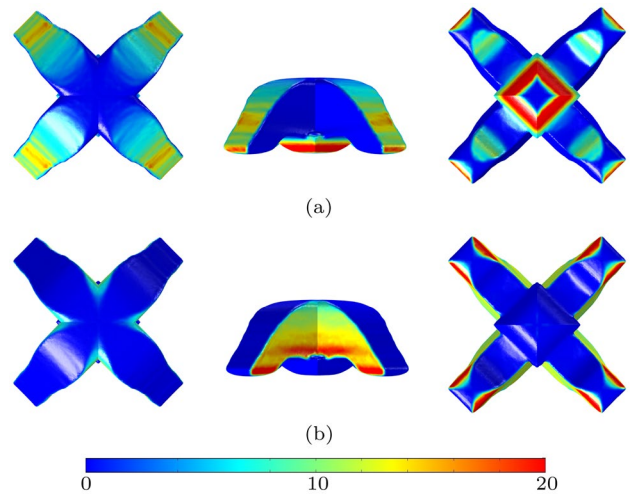


Fig. 11 Verification of the developability constraint for Fig. 10 design: **a** $(\nabla\phi \cdot \mathbf{v}^{(1)})^2$ and **b** $(\nabla\phi \cdot \mathbf{v}^{(2)})^2$

4.2 Thin-walled structure

The second example, a sheared cantilever beam, demonstrates the proposed thin-wall constraint. As seen in Fig. 5b, the design domain is subject to a shear load on an edge at the free end of the beam. The left surface is fixed in all three degrees of freedom. The maximum allowable volume fraction is set as 25%. As a baseline of comparison, the optimized design using the conventional SIMP topology optimization (without the geometric constraint) is presented in Fig. 12, which exhibits U-shaped geometry with varying cross sections. From the cross-sectional view in Fig. 12b, it can be seen that the optimized beam has no enclosed cavity with non-uniform wall thickness. The resulting structural compliance is normalized as 1.00 for comparison.

Figure 13 presents optimized designs using the proposed thin-wall constraint with three different prescribed thicknesses 0.07, 0.055, and 0.045. It is observed that the thicknesses and optimized topologies are sensitive to the selection of filter radii \bar{r} and \underline{r} , which control the minimum and maximum feature sizes, respectively. Their normalized structural compliance objective values are 1.03 (thickness = 0.07), 1.04 (thickness = 0.055) and 1.08 (thickness = 0.045), respectively. More degradation of structural performance is observed in the thinner designs, since the baseline design has relatively large (non-uniform) wall thickness. While they share the overall U-shaped geometry with the baseline, the topologies of the optimized designs are quite different from that of the baseline design, with multiply connected geometry consisting of several enclosed cavities and branched walls with near-uniform thickness. It is observed that the uniform thickness is not perfectly preserved in certain sharp corners and intersections. This

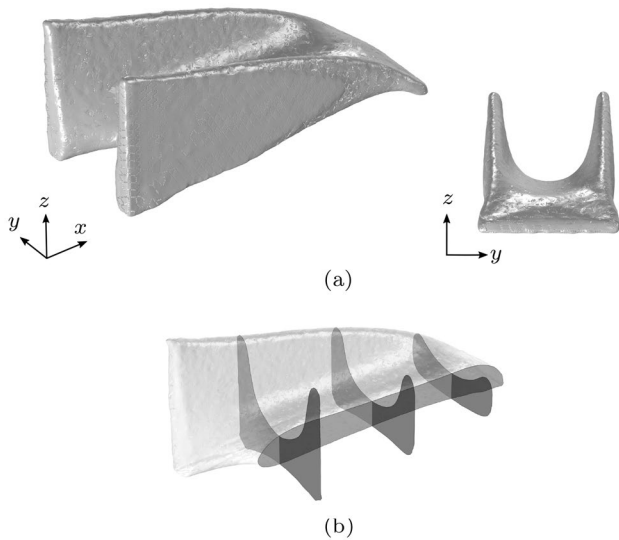


Fig. 12 Baseline structure using the conventional SIMP topology optimization. Structural compliance is 1.00 (normalized). **a** external shape with two different view angles and **b** cross-sectional view

is due to the soft constraint formulation in Eq. 11 and the selection of tuning parameters. As for intersections, the use of a ring shape test region (Fernández et al. 2019) instead of the conventional full sphere can potentially eliminate the thickness variation.

4.3 Developable thin-walled structure

The third example, a multiply loaded cube, demonstrates the integration of both the piecewise developability constraint and the thin-wall constraints. As seen in Fig. 5c, the design domain is subject to a vertical load and a shear load, which are simultaneously applied on the top face of to a cubic design domain. One of four corners of the bottom face is fixed in all three degrees of freedom while the rest are fixed only in the z direction. The upper bound on allowable volume fraction is set as 6%.

Figure 14a presents the baseline design using the conventional SIMP topology optimization (without geometric constraints), which exhibits complex free-form 3D volumetric geometry with highly variable cross sections. From the cross-sectional view, it is observed that the optimized structure consists of various geometric features typical for topology optimization with small volume fraction, e.g., beams, walls and holes. As in the earlier examples, the resulting structural compliance is normalized as 1.00 for comparison. Fig. 14b presents the optimized design using the thin-wall constraint with the prescribed thickness of 0.03. Due to the additional constraint, its normalized structural compliance increases to 1.20. As in the earlier examples, the overall geometry is similar to the baseline, with notable differences in details. The cross-sectional view reveals that certain solid beams in the baseline have become hollow and several cut-outs in the outer walls in the baseline have filled with material. Fig. 14c presents the optimized design using both the piecewise developability constraint with $\mathbf{v}^{(1)} = (1, 0, 0)$ and $\mathbf{v}^{(2)} = (0, 1, 0)$ and the thin-wall constraint with the

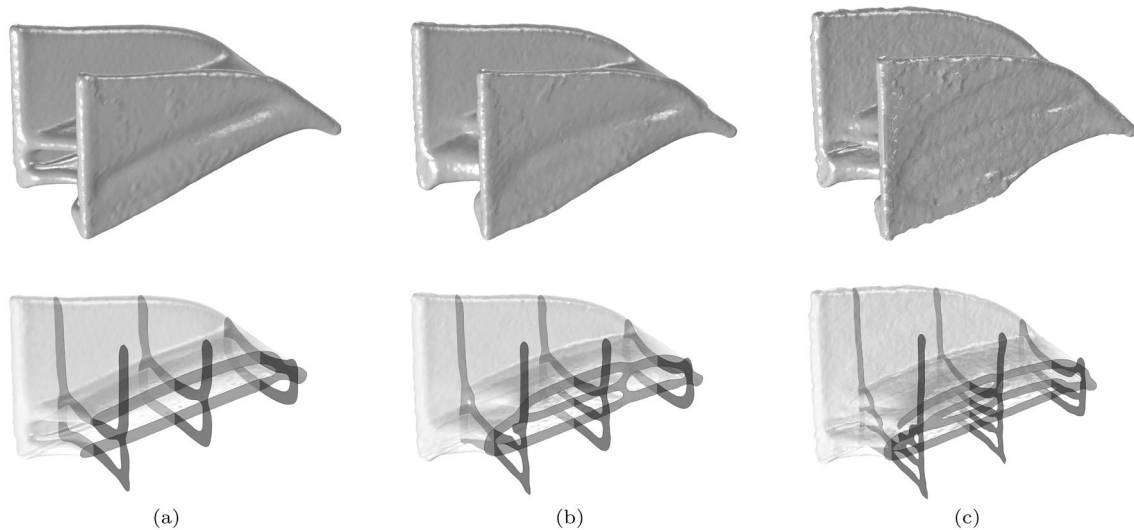


Fig. 13 Optimized structures with the thin-wall constraint with different wall thicknesses. External (top row) and cross-sectional (bottom row) views. **a** thickness = 0.07, structural compliance = 1.03 (nor-

malized); **b** thickness = 0.055, structural compliance = 1.04 (normalized); **c** thickness = 0.045, structural compliance = 1.08 (normalized)

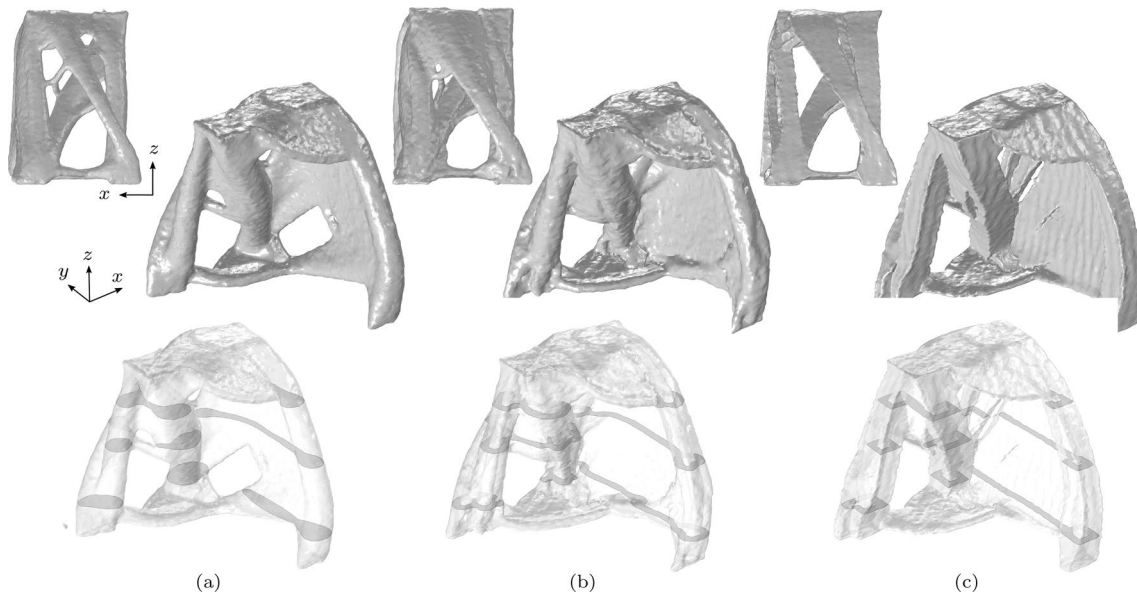


Fig. 14 Optimized designs for the multiply loaded cube example. External (top row) and cross-sectional (bottom row) views. **a** baseline design using the conventional SIMP topology optimization, struc-

tural compliance = 1.00(normalized); **b** thin-walled design, structural compliance = 1.20 (normalized); **c** developable thin-walled design, structural compliance = 1.43 (normalized)

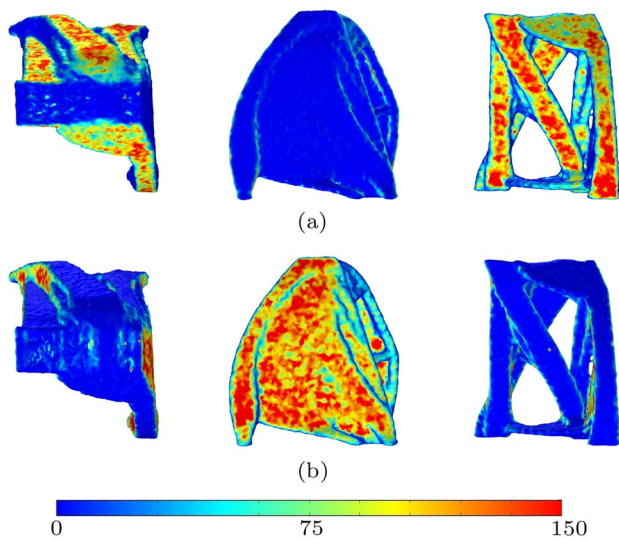


Fig. 15 Verification of the developability constraint for Fig. 14c design: **a** $(\nabla\phi \cdot \mathbf{v}^{(1)})^2$ and **b** $(\nabla\phi \cdot \mathbf{v}^{(2)})^2$

prescribed thickness of 0.03. Figure 15 verifies that the surface normal directions are perpendicular to at least one of the prescribed input vectors. Due to the two additional constraints, its normalized structural compliance further increases to 1.43. While the overall geometry is similar to the thin-walled design including hollow beams, the optimized design is made of singly curved surfaces connected by visible edges.

Table 1 Parameters used to generate Fig. 14c design

Parameter	Value	Description
P	3	SIMP power law
\bar{V}	0.06	Volume fraction constraint limit
$\bar{\epsilon}$	0.1	Developability constraint limit
$\bar{\epsilon}$	0.01	Thin-wall constraint limit
\underline{R}	0.015	Minimum filter radius
\bar{R}	0.035	Maximum filter radius
\tilde{h}	0.6 \rightarrow 0.2	Heaviside bandwidth for \tilde{H} (continuation after 30 iterations)
\bar{h}	0.2	Heaviside bandwidth for \bar{H}
\hat{h}	0.1	Heaviside bandwidth for \hat{H}
β	0.9	Threshold for the $\bar{\rho}$

Parameters used to generate Fig. 14c design are summarized in Table 1. For other examples, a similar parameter setting can be used. The optimization convergence history for Fig. 14c design is presented in Fig. 16. The compliance objective almost monotonously decreases throughout the 100 optimization iterations. The volume fraction constraint stays active from the beginning of optimization. While oscillations are observed for the two geometric constraints, both are satisfied at the end of optimization with a clear downward trend.

As relatively small volume fraction (6%) is used in this example, the design domain is adaptively re-meshed after every five optimization iterations based on the density field.

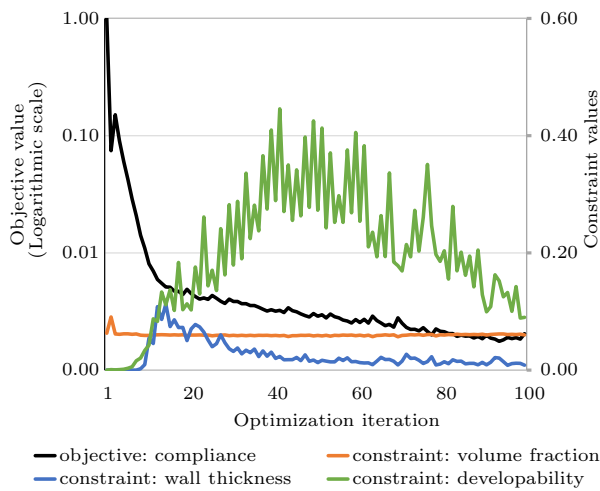


Fig. 16 Optimization convergence history for Fig. 14c design

As seen in Fig. 17 at the end of optimization, regions with higher densities (*i.e.*, structural members) have finer mesh than regions with lower densities (*i.e.*, voids).

5 Conclusions

Foldable shape-changing structures such as origami, deployable, and 4D printed structures have potentials for enhanced packaging, adaptability, and motion capabilities. Distinct geometric features often found in such foldable shape-changing structures include developability and small wall thickness. In this paper, two geometric constraints were introduced to enable the use of density-based

topology optimization in designing piecewise developable thin-walled structures. The proposed developability constraint enforces the normal directions of the surfaces of the structures to lie on a prescribed (small) number of input reference planes, which realizes an optimized structure made of piecewise developable surfaces. While this conservative constraint only imposes the sufficient condition for piecewise developability, it is far more computationally efficient than a necessary and sufficient constraint based on the Gaussian curvature, which makes it highly suitable for use with density-based topology optimization. The proposed thin-wall constraint simultaneously bounds the minimum and the maximum feature sizes in the structures through two PDE-based filtering operations and an aggregation constraint. While these additional constraints inevitably compromise the structural performance, the ability to control the desired geometric features in topology optimization would benefit the rapidly growing field of foldable shape-changing structures.

Due to the intrinsic characteristics of the density-based representation and the associated computational cost, however, the “thin”-walled designs presented in this paper still all have relatively thick walls. To further reduce the thickness in thin-walled designs, adaptive switching from solid to shell elements (Träff et al. 2021) during optimization might be beneficial. In addition, designing foldable shape-changing structures imposes the requirements beyond the piecewise developability and small wall thickness addressed in this paper. Such requirements include designing for the folding sequence and avoiding self-overlaps in the developed (flattened) sheet as well as the potential use of multiple sheets. Addressing these issues are left for the future work.

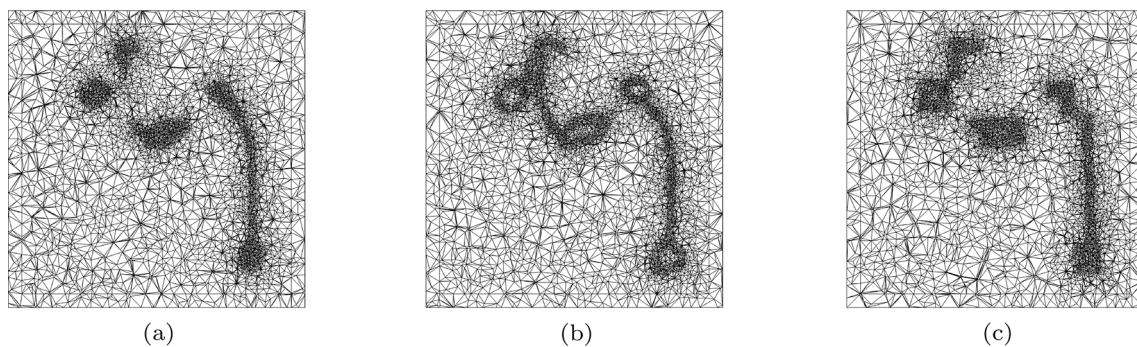


Fig. 17 Mesh of the mid-plane ($z = 0.5$) at the end of optimization for **a** baseline, **b** thin-walled, and **c** developable thin-walled designs in Fig. 14

Declarations

Conflict of interest The authors have no conflict of interest in the preparation or publication of this work.

Replication of Results Due to institutional constraints, the source code is unavailable. However, further algorithm details are available upon request to the authors.

References

- Aumann G (2004) Degree elevation and developable Bézier surfaces. *Comput Aided Geom Des* 21:661
- Bendsoe MP, Sigmund O (2003) *Topology optimization: theory, methods, and applications*. Springer Science & Business Media, New York
- Bruns TE, Tortorelli DA (2001) Topology optimization of non-linear elastic structures and compliant mechanisms. *Comput Methods Appl Mech Eng* 190:3443
- Carstensen JV, Guest JK (2018) Projection-based two-phase minimum and maximum length scale control in topology optimization. In: *Structural and multidisciplinary optimization*, pp 1–16
- Chu C-H, Séquin CH (2002) Developable Bézier patches: properties and design. *Comput Aided Des* 34:511
- Clausen A, Aage N, Sigmund O (2015) Topology optimization of coated structures and material interface problems. *Comput Methods Appl Mech Eng* 290:524
- Clausen A, Andreassen E, Sigmund O (2015) Topology optimization for coated structures. In: Li Q, Steven GP, Zhang Z (eds) *Proceedings of the 11th world congress on structural and multidisciplinary optimization*, pp 7–12
- Cozmei M, Hasseler T, Kinyon E, Wallace R, Deleo AA, Salviato M (2020) Aerogami: composite origami structures as active aerodynamic control. *Compos B Eng* 184:107719
- Deleo AA, O'Neil J, Yasuda H, Salviato M, Yang J (2020) Origami-based deployable structures made of carbon fiber reinforced polymer composites. *Compos Sci Technol* 191:108060
- Dienemann R, Schumacher A, Fiebig S (2017) Topology optimization for finding shell structures manufactured by deep drawing. *Struct Multidisc Optim* 56:473
- Elber G (1995) Model fabrication using surface layout projection. *Comput Aided Des* 27:283
- Fernández E, Collet M, Alarcón P, Bauduin S, Duysinx P (2019) An aggregation strategy of maximum size constraints in density-based topology optimization. *Struct Multidisc Optim* 60:2113
- Goldman R (2005) Curvature formulas for implicit curves and surfaces. *Comput Aided Geom Des* 22:632
- Guest JK (2009) Imposing maximum length scale in topology optimization. *Struct Multidisc Optim* 37:463
- Guest JK, Prévost JH, Belytschko T (2004) Achieving minimum length scale in topology optimization using nodal design variables and projection functions. *Int J Numer Meth Eng* 61:238
- Hoschek J (1998) Approximation of surfaces of revolution by developable surfaces. *Comput Aided Des* 30:757
- Ion A, Rabinovich M, Herholz P, Sorkine-Hornung O (2020) Shape approximation by developable wrapping. *ACM Trans Graph (TOG)* 39:1
- Jiang C, Wang C, Rist F, Wallner J, Pottmann H (2020) Quad-mesh based isometric mappings and developable surfaces. *ACM Trans Graph (TOG)* 39:128
- Julius D, Kraevoy V, Sheffer A (2005) D-charts: quasi-developable mesh segmentation. *Comput Graph Forum* 24:581
- Kawamoto A, Matsumori T, Yamasaki S, Nomura T, Kondoh T, Nishiwaki S (2011) Heaviside projection based topology optimization by a PDE-filtered scalar function. *Struct Multidisc Optim* 44:19
- Kilian M, Flöry S, Chen Z, Mitra NJ, Sheffer A, Pottmann H (2008) Curved folding. *ACM Trans Graph* 27:75
- Kühnel W (2015) *Differential geometry*, vol 77. American Mathematical Soc, New York
- Laccone F, Malomo L, Pietroni N, Cignoni P, Schork T (2021) Integrated computational framework for the design and fabrication of bending-active structures made from flat sheet material. *Structures* 34:979–994
- Lang J, Röschel O (1992) Developable (1, n)-Bézier surfaces. *Comput Aided Geom Des* 9:291
- Lazarov BS, Sigmund O (2011) Filters in topology optimization based on Helmholtz-type differential equations. *Int J Numer Method Eng* 86:765
- Lazarov BS, Wang F (2017) Maximum length scale in density based topology optimization. *Comput Methods Appl Mech Eng* 318:826
- Liu Y, Pottmann H, Wallner J, Yang Y-L, Wang W (2006) Geometric modeling with conical meshes and developable surfaces. *ACM Trans Graph* 25:681
- Massarwi F, Elber G, Gotsman C (2007) Papercraft models using generalized cylinders. In: *Computer graphics and applications, pacific conference on (PG) (IEEE)*, pp 148–157
- Mitani J, Suzuki H (2004) Making papercraft toys from meshes using strip-based approximate unfolding. *ACM Trans Graph* 23:259
- Niu B, Wadbro E (2019) On equal-width length-scale control in topology optimization. *Struct Multidisc Optim* 59:1321
- Nomura T, Kawamoto A, Kondoh T, Dede EM, Lee J, Song Y, Kikuchi N (2019) Inverse design of structure and fiber orientation by means of topology optimization with tensor field variables. *Compos B Eng* 176:107187
- Pottmann H, Schiftner A, Bo P, Schmiedhofer H, Wang W, Baldassini N, Wallner J (2008) Freeform surfaces from single curved panels. *ACM Trans Graph* 27:76
- Pottmann H, Farin G (1995) Developable rational Bézier and B-spline surfaces. *Comput Aided Geom Des* 12:513
- Poulsen TA (2003) A new scheme for imposing a minimum length scale in topology optimization. *Int J Numer Meth Eng* 57:741
- Pérez F, Suárez JA (2007) Quasi-developable B-spline surfaces in ship hull design. *Comput Aided Des* 39:853
- Rabinovich M, Hoffmann T, Sorkine-Hornung O (2018) Discrete geodesic nets for modeling developable surfaces. *ACM Trans Graph (TOG)* 37:1
- Redoutey M, Roy A, Filipov ET (2021) Pop-up kirigami for stiff, dome-like structures. *Int J Solids Struct* 229:111140
- Rose K, Sheffer A, Wither J, Cani M-P, Thibert B (2007) Developable surfaces from arbitrary sketched boundaries. In: *SGP'07-5th Eurographics symposium on geometry processing (Eurographics Association)*, pp 163–172
- Shatz I, Tal A, Leifman G (2006) Paper craft models from meshes. *Vis Comput* 22:825
- Sigmund O (1997) On the design of compliant mechanisms using topology optimization. *J Struct Mech* 25:493
- Sigmund O (2007) Morphology-based black and white filters for topology optimization. *Struct Multidisc Optim* 33:401
- Solomon J, Vouga E, Wardetzky M, Grinspun E (2012) Flexible developable surfaces. *Comput Graph Forum* 31:1567
- Stein O, Grinspun E, Crane K (2018) Developability of triangle meshes. *ACM Trans Graph* 37:77
- Svanberg K (1987) The method of moving asymptotes—a new method for structural optimization. *Int J Numer Method Eng* 24:359
- Tahouni Y, Cheng T, Wood D, Sachse R, Thierer R, Bischoff M, Menges A (2020) Self-shaping curved folding: A 4D-printing

- method for fabrication of self-folding curved crease structures. In: Symposium on computational fabrication, pp 1–11
- Tang C, Bo P, Wallner J, Pottmann H (2016) Interactive design of developable surfaces. *ACM Trans Graph* 35:12
- Träff EA, Sigmund O, Aage N (2021) Topology optimization of ultra high resolution shell structures. *Thin Walled Struct* 160:107349
- Wang C, Qian X (2018) Heaviside projection-based aggregation in stress-constrained topology optimization. *Int J Numer Meth Eng* 115:849
- Wu J, Aage N, Westermann R, Sigmund O (2018) Infill optimization for additive manufacturing—approaching bone-like porous structures. *IEEE Trans Visual Comput Graphics* 24:1127
- Wu J, Clausen A, Sigmund O (2017) Minimum compliance topology optimization of shell-infill composites for additive manufacturing. *Comput Methods Appl Mech Eng* 326:358
- Zhang S, Gain AL, Norato JA (2017) Stress-based topology optimization with discrete geometric components. *Comput Methods Appl Mech Eng* 325:1
- Zhang S, Gain AL, Norato JA (2018) A geometry projection method for the topology optimization of curved plate structures with placement bounds. *Int J Numer Meth Eng* 114:128
- Zhang S, Norato JA, Gain AL, Lyu N (2016) A geometry projection method for the topology optimization of plate structures. *Struct Multidisc Optim* 54:1173
- Zhang W, Zhong W, Guo X (2014) An explicit length scale control approach in SIMP-based topology optimization. *Comput Methods Appl Mech Eng* 282:71
- Zhou M, Lazarov BS, Wang F, Sigmund O (2015) Minimum length scale in topology optimization by geometric constraints. *Comput Methods Appl Mech Eng* 293:266
- Zhou Y, Nomura T, Saitou K (2021) Anisotropic multicomponent topology optimization for additive manufacturing with build orientation design and stress-constrained interfaces. *J Comput Inform Sci Eng* 21:011007

Publisher's Note Springer Nature remains neutral with regard to jurisdictional claims in published maps and institutional affiliations.